RESEARCH ARTICLE

CREBBP Inactivation Promotes the Development of HDAC3-Dependent Lymphomas

Yanwen Jiang[1,2], Ana Ortega-Molina[3], Huimin Geng[4], Hsia-Yuan Ying[1], Katerina Hatzi[1,3], Sara Parsa[3], Dylan McNally[1], Ling Wang[1], Ashley S. Doane[2], Xabier Agirre[1,5], Matt Teater[2], Cem Meydan[2], Zhuoning Li[1], David Poloway[1], Shenqiu Wang[3], Daisuke Ennishi[6], David W. Scott[6], Kristy R. Stengel[7], Janice E. Kranz[8], Edward Holson[8], Sneh Sharma[9], James W. Young[10], Chi-Shuen Chu[11], Robert G. Roeder[11], Rita Shaknovich[12], Scott W. Hiebert[7], Randy D. Gascoyne[6], Wayne Tam[13], Olivier Elemento[2], Hans-Guido Wendel[3], and Ari M. Melnick[1]

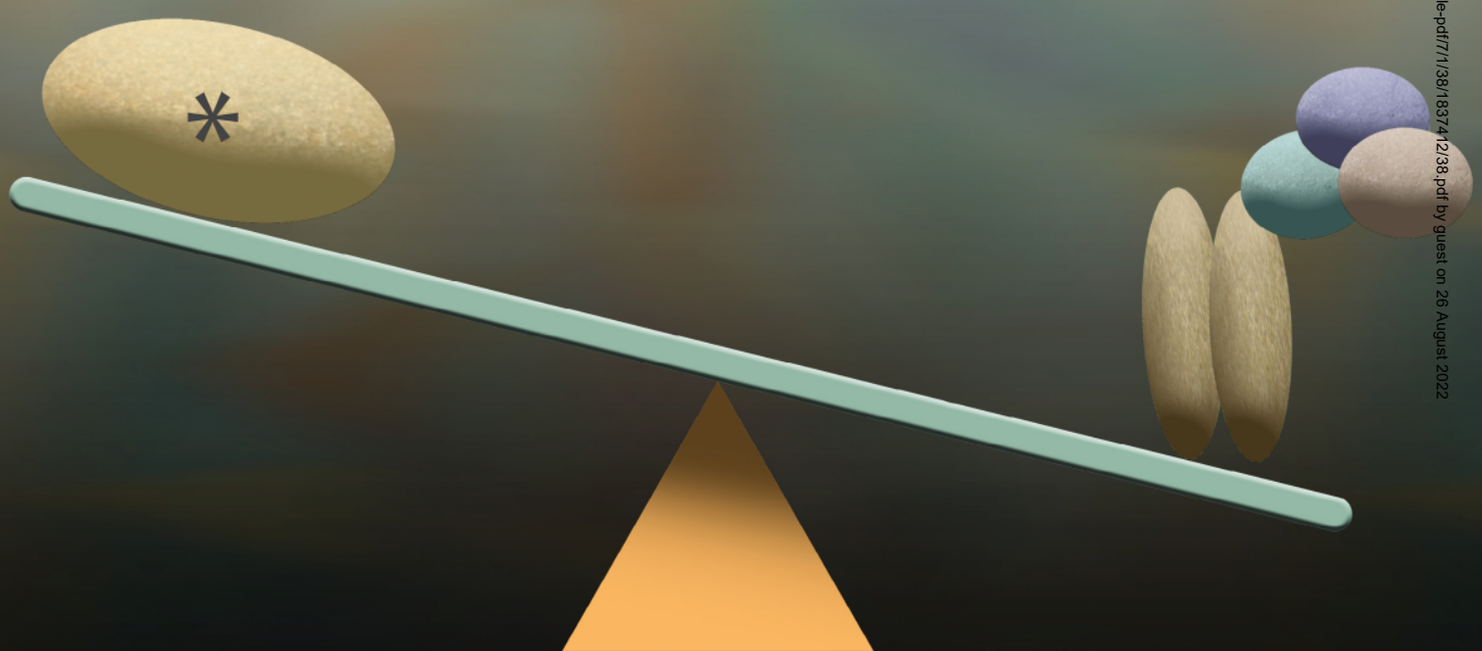

ABSTRACT Somatic mutations in *CREBBP* occur frequently in B-cell lymphoma. Here, we show that loss of CREBBP facilitates the development of germinal center (GC)–derived lymphomas in mice. In both human and murine lymphomas, CREBBP loss-of-function resulted in focal depletion of enhancer H3K27 acetylation and aberrant transcriptional silencing of genes that regulate B-cell signaling and immune responses, including class II MHC. Mechanistically, CREBBP-regulated enhancers are counter-regulated by the BCL6 transcriptional repressor in a complex with SMRT and HDAC3, which we found to bind extensively to MHC class II loci. HDAC3 loss-of-function rescued repression of these enhancers and corresponding genes, including MHC class II, and more profoundly suppressed *CREBBP*-mutant lymphomas *in vitro* and *in vivo*. Hence, CREBBP loss-of-function contributes to lymphomagenesis by enabling unopposed suppression of enhancers by BCL6/SMRT/HDAC3 complexes, suggesting HDAC3-targeted therapy as a precision approach for *CREBBP*-mutant lymphomas.

SIGNIFICANCE: Our findings establish the tumor suppressor function of CREBBP in GC lymphomas in which *CREBBP* mutations disable acetylation and result in unopposed deacetylation by BCL6/SMRT/HDAC3 complexes at enhancers of B-cell signaling and immune response genes. Hence, inhibition of HDAC3 can restore the enhancer histone acetylation and may serve as a targeted therapy for *CREBBP*-mutant lymphomas. *Cancer Discov; 7(1); 38–53. ©2016 AACR.*

See related commentary by Höpken, p. 14.

INTRODUCTION

Follicular lymphoma and diffuse large B-cell lymphoma (DLBCL) are the two most common subtypes of non-Hodgkin lymphoma (NHL). Although initially exhibiting an indolent phenotype, follicular lymphomas are nevertheless mostly incurable, and 40%–50% eventually transform into an aggressive and lethal form of DLBCL (1). DLBCLs manifest an aggressive and fast-growing phenotype, but can be eradicated by chemoimmunotherapy (R-CHOP) in approximately 60% of cases. Both follicular lymphoma and DLBCLs arise from B cells undergoing the germinal center (GC) reaction, a stage of the humoral immune response where B cells undergo immunoglobulin affinity maturation. GC B cells form transiently in response to T-cell–dependent antigen stimulation and are characterized by their unique ability to simultaneously proliferate and tolerate genomic instability. These features make these cells inherently prone to malignant transformation.

Genome-sequencing studies have shown that the recurrent mutation of histone-modifying enzymes is a genetic hallmark of follicular lymphoma and DLBCL. Some of the most highly recurrent disease alleles in follicular lymphoma and DLBCL correspond to somatic mutation affecting two closely related histone acetyltransferase (HAT)–encoding genes: *CREBBP* and *EP300*. Between these two loci, *CREBBP* somatic mutations are more frequent, reported in 6.4%–22.3% of patients with DLBCL and 30.8%–68% of follicular lymphomas (2–7). These mutations are frequently monoallelic and tend to occur within the HAT enzymatic domain. HAT domain missense mutants may lose their ability to acetylate protein substrates, such as histones or transcription factors, due to reduced binding of acetyl-CoA (2). Mutations in *EP300* occur in 5.4%–9.7% of DLBCLs and 8.7%–23.1% of follicular lymphomas (2, 3, 6, 7),

[1]Department of Medicine and Weill Cornell Cancer Center, Weill Cornell Medicine, New York, New York. [2]Institute for Computational Biomedicine, Weill Cornell Medical College, New York, New York. [3]Cancer Biology and Genetics Program, Memorial Sloan Kettering Cancer Center, New York, New York. [4]Department of Laboratory Medicine, University of California, San Francisco, San Francisco, California. [5]Area de Oncología, Centro de Investigación Médica Aplicada (CIMA), Universidad de Navarra, Pamplona, Spain. [6]Centre for Lymphoid Cancer, British Columbia Cancer Agency, Vancouver, British Columbia, Canada. [7]Department of Biochemistry, Vanderbilt University School of Medicine, Nashville, Tennessee. [8]KDAc Therapeutics, Cambridge, Massachusetts. [9]Laboratory of Cellular Immunobiology, Division of Hematologic Oncology, Department of Medicine, Memorial Sloan Kettering Cancer Center, New York, New York. [10]Laboratory of Cellular Immunobiology, Division of Hematologic Oncology, Department of Medicine, Memorial Sloan Kettering Cancer Center, Weill Cornell Medicine; The Rockefeller University, New York, New York. [11]Laboratory of Biochemistry and Molecular Biology, The Rockefeller University, New York, New York. [12]Cancer Genetics Incorporated, Rutherford, New Jersey. [13]Department of Pathology and Laboratory Medicine, Weill Cornell Medicine, New York, New York.

Note: Supplementary data for this article are available at Cancer Discovery Online (http://cancerdiscovery.aacrjournals.org/).

Y. Jiang, A. Ortega-Molina, H. Geng, and H.-Y. Ying contributed equally to this article.

Current address for Y. Jiang: Genentech, South San Francisco, CA; current address for A. Ortega-Molina, Metabolism and Cell Signaling Group, Spanish National Cancer Research Centre (CNIO), Madrid, Spain. J.E. Kranz is a former employee of KDAc Therapeutics.

Corresponding Authors: Ari M. Melnick, Weill Cornell Medicine, 413 E 69th Street, BB-1430, New York, NY 10021. Phone: 646-962-6725; Fax: 212-746-8866; E-mail: amm2014@med.cornell.edu; and Hans-Guido Wendel, Memorial Sloan Kettering Cancer Center, 1275 York Avenue, New York, NY 10065. Phone: 646-888-2526; Fax: 646-422-0197; E-mail:wendelh@mskcc.org

doi: 10.1158/2159-8290.CD-16-0975

and are often mutually exclusive with those of *CREBBP*, suggesting that loss of either of these two genes might affect a common downstream pathway. It is not yet known how these mutations might contribute to malignant transformation. Notably, *CREBBP* mutations tend to be early events in lymphomagenesis, and, for example, in follicular lymphoma, likely occur in B cells that already harbor the t(14;18) translocation that drives constitutive expression of BCL2 (7).

CREBBP mediates acetylation of certain histone lysine residues, and among these the best characterized from the functional standpoint is H3K27 acetylation (H3K27ac), which is required for the activation of enhancers. Enhancers are largely responsible for cell context–specific transcriptional programming, and are located at sites distal to gene-coding regions or within introns. For a genomic region to manifest enhancer activity, it must acquire H3K4 mono/dimethylation (H3K4me1/2; ref. 8). However, for enhancers to become fully active, they require the further addition of H3K27ac mark by HATs such as CREBBP and EP300 (9). Therefore, it is possible that loss of CREBBP and EP300 HAT activity may disrupt the activity of enhancers in B cells, and perhaps through this mechanism contributes to lymphomagenesis. Such an effect has been suggested by several recent reviews (10, 11). In this study, we explore the role and epigenetic mechanism of action of CREBBP in lymphomagenesis.

RESULTS

Crebbp Deficiency Promotes Lymphomagenesis *In Vivo*

Although *CREBBP* mutations are among the most frequent genetic lesions in NHL, their functional significance is unknown. We modeled CREBBP deficiency in VavP-*Bcl2* transgenic mice, which closely recapitulate the genetics and pathology of human follicular lymphoma (12–14). Vav*Bcl2* hematopoietic progenitor cells (HPC) were transduced with GFP-encoding retroviruses expressing shRNAs against *Crebbp* (VavP-*Bcl2/Crebbp*^{KD}) or control (VavP-*Bcl2/GFP*), and transplanted into lethally irradiated wild-type (WT) recipients (Supplementary Fig. S1A). *Crebbp* shRNAs induced robust knockdown of *Crebbp* expression measured by RT-qPCR in murine FL5-12 cells (Supplementary Fig. S1B). We observed a significant acceleration of lymphoma onset in VavP-*Bcl2/Crebbp*^{KD} (shRNA #1, $n = 34$, $P = 0.0465$) as compared with VavP-*Bcl2/GFP* group ($n = 31$, Fig. 1A). This was reproduced with a second shRNA (shRNA #3, Supplementary Fig. S1C). The contribution of CREBBP was evident in that only 13% to 19% of HPCs expressed GFP, whereas 90% of lymphoma cells were GFP$^+$ in the VavP-*Bcl2/Crebbp*^{KD} (Fig. 1B). Overall VavP-*Bcl2/Crebbp*^{KD} tumors contained a significantly higher ratio of transduced cells than VavP-*Bcl2/GFP* tumors ($P = 0.01$, Mann–Whitney *U* test, Fig. 1C). We purified B220$^+$ lymphoma cells from the spleen and examined the global H3K27ac level by Western blotting. We observed that acetylation of H3K27 was reduced in lymphoma cells transduced with *Crebbp* shRNA, confirming the functional impact of *Crebbp* knockdown (Supplementary Fig. S1D). The lymphoma cells from VavP-*Bcl2/Crebbp*^{KD} were B220$^+$, CD19$^+$, IgM$^+$, and CD3$^-$ (Fig. 1D; Supplementary Fig. S1E), confirming their B-cell identity. VavP-*Bcl2/Crebbp*^{KD} lymphomas were more aggressive and widely disseminated than VavP-*Bcl2* control tumors, as shown by scoring tissue invasion and disease morphology by histopathology of the spleen and other organs (Fig. 1D and E; Supplementary Fig. S1F). PCR analysis of the murine IgL V_λ-J_λ locus indicated that these lymphomas were clonal (Supplementary Fig. S1G). Somatic hypermutation is a hallmark of GC B cells and GC-derived lymphomas (15). Indeed, sequencing the VDJH4 locus of both VavP-*Bcl2/Crebbp*^{KD} and VavP-*Bcl2* control lymphomas revealed the presence of somatic hypermutation, confirming the GC origin of these tumors (Supplementary Fig. S1H). A similar general phenotype was observed using shRNA against *Ep300* in VavP-*Bcl2* transgenic mice, including the significant acceleration of lymphoma onset ($n = 37$, $P = 0.0143$, log-rank test), more aggressive histology, B-cell immunophenotype, clonality, and GC origin (Supplementary Fig. S2). Hence, *Crebbp* and *Ep300* deficiency can promote GC lymphomagenesis and function as tumor suppressor genes.

Crebbp Deficiency Leads to Preferential Loss of H3K27ac at Enhancers

For downstream mechanistic studies exploring how loss of histone acetyl transferases could accelerate lymphomagenesis, we focused primarily on *Crebbp,* as (i) *Crebbp* KD and *Ep300* KD resulted in similar phenotype, (ii) *CREBBP* mutations are more frequent in humans, and (iii) *CREBBP* mutations are mutually exclusive with *EP300*, suggesting overlapping mechanisms of action. To determine the impact of CREBBP loss-of-function on H3K27 acetylation patterning, we performed chromatin immunoprecipitation sequencing (ChIP-seq) for H3K27ac in B220$^+$ lymphoma cells from VavP-*Bcl2/GFP* mice ($n = 4$), as well as in VavP-*Bcl2/Crebbp*^{KD} ($n = 6$) mice. We identified 18,614 H3K27ac "peaks" in VavP-*Bcl2/GFP* lymphomas (Fig. 2A). Interestingly, there was a net loss of 3,660 (19.7%) peaks and practically zero gain of new peaks in VavP-*Bcl2/Crebbp*^{KD} lymphomas (Fig. 2A). A similar effect was observed in human GC–derived lymphoma B cells where *CREBBP* was depleted using two independent shRNAs, with focal loss of 17.3% of H3K27ac peaks after *CREBBP* knockdown (Fig. 2A; Supplementary Fig. S3A). As in the mice, depletion of *CREBBP* in the human cells also resulted in global reduction of H3K27ac (Supplementary Fig. S3B).

We focused on H3K27ac sites disproportionately affected by CREBBP loss-of-function as these would be most strongly linked to the functional impact. In human lymphoma cells, we observed that 76.9% of CREBBP-binding sites are located at putative enhancers, including introns, and distal regions (Supplementary Fig. S3C). Accordingly, we observed that H3K27ac peaks lost in VavP-*Bcl2/Crebbp*^{KD} lymphomas were disproportionately located at intergenic or intronic locations corresponding to putative enhancers ($P < 2.2e{-}16$, Fig. 2B), whereas unaffected peaks were preferentially located at promoters. Similarly, ChIP-seq studies in human cells indicated preferential loss of H3K27ac at putative enhancers (59.2% vs. 37.6% at promoters, $P < 2.2e{-}16$, Fig. 2B). Confirming this assessment, quantitative assessment of H3K27ac ChIP-seq profiles revealed increasing skewing toward enhancers among sites with progressively greater loss of H3K27ac after CREBBP loss-of-function in murine and human lymphoma cells ($P < 2.2e{-}16$; Fig. 2C–F; examples shown in Fig. 2G and H), and expression of genes near these enhancers was reduced in *CREBBP*-deficient cells, as determined by RNA sequencing (RNA-seq) performed in both the murine and human

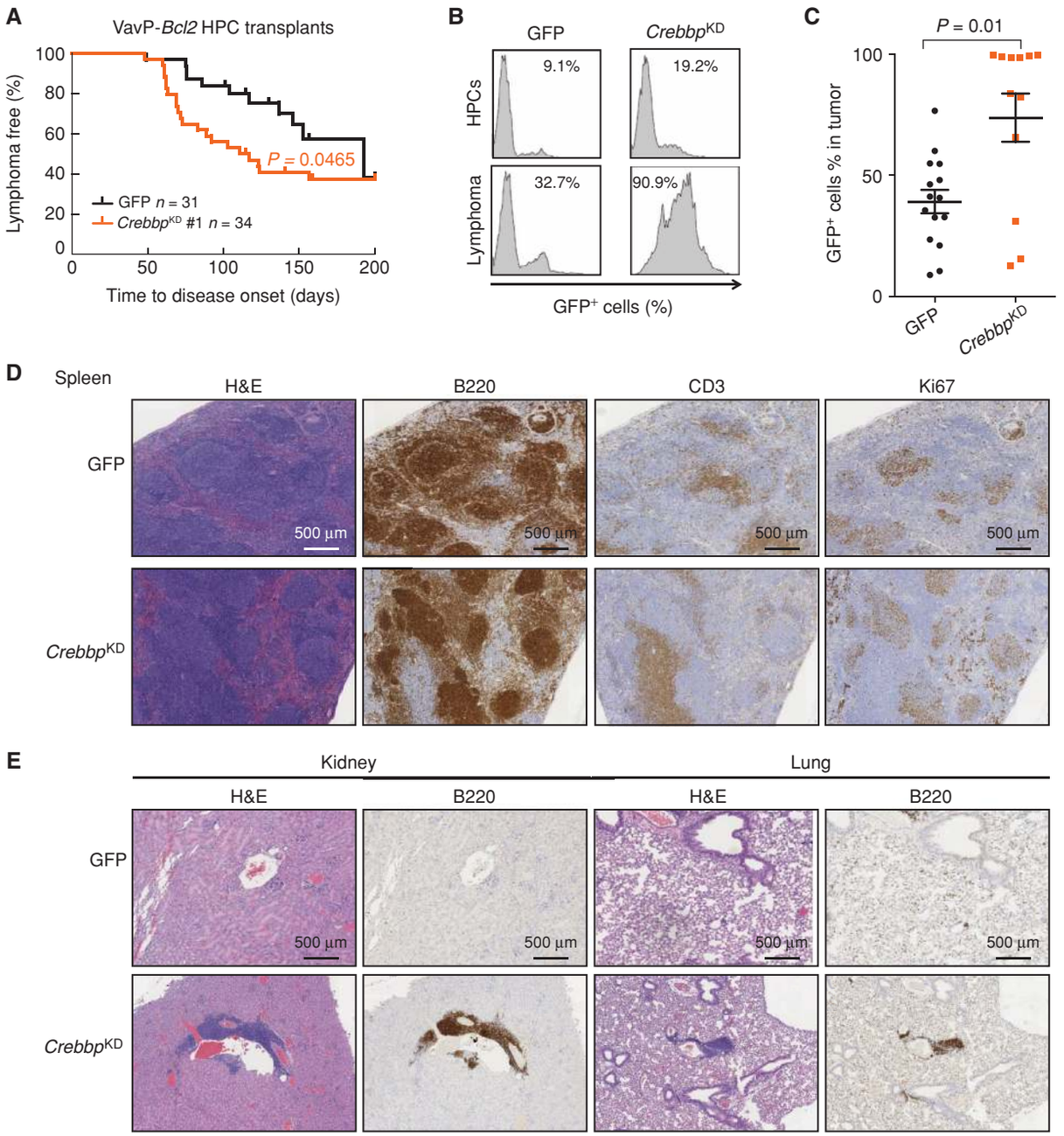

Figure 1. *Crebbp* deficiency accelerates B-cell lymphoma development in mice. **A,** Kaplan–Meier curve of C57BL/6 mice transplanted with VavP-*Bcl2* HPCs transduced with MSCV-GFP retroviral vector alone (GFP, black, $n = 31$), or containing shRNAs against *Crebbp* (red, $n = 34$). Statistical significance of survival difference was determined by the log-rank test between sh*Crebbp* and vector alone. **B,** Representative flow cytometry histograms showing the GFP-positive cell percentage of the preinjection HPCs and the splenic murine lymphoma cells that derived from the same HPCs. **C,** Dot plot representing the GFP-positive cell percentage in the splenic murine lymphoma cells in individual recipient animal. The mean and SEM were represented for each transplant group. Statistical significance was determined by Mann–Whitney test. **D,** Hematoxylin and eosin (H&E), B220, CD3, and Ki67 staining of spleen tissues extracted from recipient mice upon sacrifice. **E,** H&E and B220 staining of kidney and lung tissues extracted from recipient mice upon sacrifice.

CREBBP knockdown systems (Supplementary Fig. S4A and S4B). We did not observe significant correlation between gene expression reduction and promoter H3K27ac loss in mice, although there was a correlation in humans (data not shown), so that the enhancer effects were the most consistent effects of CREBBP loss-of-function. Finally, there was a significant enrichment of the murine CREBBP enhancer H3K27ac loss gene signature in human lymphoma cell enhancer H3K27ac loss genes with *CREBBP* knockdown ($P = 6.88e{-}23$; Fig. 2I), supporting the human relevance of the murine model. Hence, CREBBP loss-of-function preferentially affects H3K27 acetylation at enhancers and affects similar genes in humans and mice.

CREBBP Loss-of-Function Represses Enhancers that Are Poised in GC B cells

To determine more precisely how CREBBP loss-of-function perturbs enhancer function, we next mapped the location of enhancers in primary human GC B cells, which are the cell-of-origin of DLBCL and follicular lymphoma. To identify the enhancers relevant and specific to this cell type, we performed replicate ChIP-seq for H3K4me2, H3K4me3, and H3K27ac in purified primary human naïve B cells (NBC) and GC B cells. We identified 7,577 active enhancer H3K4me2$^+$H3K4me3$^-$H3K27ac$^+$ peaks in NBCs and 5,219 in GC B cells (Supplementary Fig. S5A), the great majority (two thirds) of which were unique and specific to each cell type. Changes in enhancer activation state were accompanied by corresponding changes in gene expression (Supplementary Fig. S5B and S5C; examples are shown in Supplementary Fig. S5D). Notably, among sites that lose H3K27 acetylation after *CREBBP* knockdown in mouse and human lymphomas, there was a significant enrichment for genes that also lose enhancer activity in GC B cells (Fig. 2I). Hence, CREBBP loss-of-function strengthens the repression of B-cell enhancers that are deactivated in GCs. This could contribute to lymphomagenesis by aberrantly maintaining the aspects of the GC phenotype. Indeed, further analysis of CREBBP ChIP-seq and RNA-seq signatures in mice and humans revealed significant enrichment for genes linked to termination of the GC reaction, such as those induced by CD40, IRF4 signaling, and plasma cell differentiation (Fig. 2I; Supplementary Fig. S6; for a complete list of enriched pathways, please check Supplementary Tables S1 and S2). In the human cells, we also observed enrichment for antigen presentation and MHC class II genes. This result is consistent with the reported downregulation of these genes in *CREBBP*-mutant follicular lymphomas (7). CREBBP loss-of-function thus results in a failure to activate genes involved in the GC exit and immune recognition.

To probe CREBBP function, we compared *CREBBP* knockdown RNA-seq and H3K27ac ChIP-seq profiles in mice and human cells to a database of B-cell ChIP-seq and transcriptional profiles. This approach revealed a striking enrichment for genes whose enhancers are bound by the BCL6/SMRT transcriptional repressor complex, and accordingly, genes found to be derepressed upon *BCL6* knockdown in GC-derived DLBCL cells (Fig. 2I; Supplementary Fig. S6). CREBBP and EP300 target genes in DLBCL were similarly enriched (Fig. 2I; Supplementary Fig. S6), consistent with EP300 and CREBBP having similar functions in these cells. In contrast, plasma cell genes and IRF4 signaling genes were not significantly enriched in the genes whose promoters lost H3K27ac enrichment in murine VavP-*Bcl2/Crebbp*^{KD} lymphoma cells (Supplementary Fig. S7). Taken together, these data indicate that CREBBP/EP300 and BCL6/SMRT complexes have opposing effects on enhancers that are silenced in GC B cells and are activated upon GC exit and antigen presentation.

BCL6 has not been previously implicated in antigen and MHC class II presentation; therefore, we analyzed BCL6 and SMRT ChIP-seq profiles performed in primary human naïve and GC B cells for MHC class II enhancer binding. We readily identified multiple binding sites in enhancers for MHC class II (Fig. 2J) and related genes such as *CD74* and *CIITA* (Supplementary Fig. S8). Notably, the H3K27ac level at these enhancers was reduced in GC B cells as compared with that

Figure 2. *Crebbp* deficiency results in focal H3K27ac loss in mouse and human lymphoma. **A,** Venn diagrams showing the overlap between the H3K27ac peaks in B220$^+$ cells from VavP-*Bcl2*/GFP tumors ($n = 4$) or from VavP-*Bcl2*/sh*Crebbp* tumors ($n = 6$; left), or the overlap between the H3K27ac peaks in MD901 cells transduced with either control scramble shRNA ($n = 3$) or shRNAs against *CREBBP* ($n = 6$; right). **B,** Stacked bar plot representing the genomic distribution of common and lost H3K27ac peaks between VavP-*Bcl2*/GFP and VavP-*Bcl2*/sh*Crebbp* tumor cells (left), or between MD901 cells transduced with either control scramble or *CREBBP* shRNAs ($n = 6$). **C,** Normalized average H3K27ac read density plot at loci identified as H3K27ac peaks in MACS-purified B220$^+$ B cells from VavP-*Bcl2*/GFP tumors. The black line represents the average values in VavP-*Bcl2*/EV tumors ($n = 4$), and the dark red line represents the values in VavP-*Bcl2*/sh*Crebbp* tumors ($n = 6$). Average values of peaks that exhibited more than 25%, 35%, 40%, and 50% reads loss in VavP-*Bcl2*/sh*Crebbp* tumors as compared with VavP-*Bcl2*/GFP tumors are shown as lines in different shades of red. *, statistically significant loss of normalized H3K27ac read density as determined by Kolmogorov–Smirnov test. **D,** Bar plot representing ratio of the proportions of enhancer peaks or promoter peaks that exhibited more than 25%, 35%, 40%, and 50% reads loss in VavP-*Bcl2*/sh*Crebbp* tumors as compared with VavP-*Bcl2*/GFP tumors. **E,** Normalized average H3K27ac read density plot at loci identified as H3K27ac peaks in scramble shRNA–transduced MD901 cells. The black line represents the average values in scramble shRNA transduced MD901 cells ($n = 3$), and the dark red line represents the values in *CREBBP* shRNAs transduced MD901 cells ($n = 6$). Average values of peaks that exhibited more than 25%, 40%, 50%, and 70% reads loss in *CREBBP* KD cells as compared with control scramble cells are shown as lines in different shades of red. *, statistically significant loss of normalized H3K27ac read density as determined by Kolmogorov–Smirnov test. **F,** Bar plot representing ratio of the proportions of enhancer peaks or promoter peaks that exhibited more than 25%, 40%, 50%, and 70% reads loss in *CREBBP* KD cells as compared with control scramble MD901 cells. **G,** UCSC read-density tracks of normalized H3K27ac ChIP-seq reads at murine *Cd86* locus in two representative VavP-*Bcl2*/GFP tumors and two representative VavP-*Bcl2*/sh*Crebbp* tumors. Shaded areas highlight the regions showing loss of H3K27ac in VavP-*Bcl2*/sh*Crebbp* tumors. **H,** UCSC read-density tracks of normalized H3K27ac ChIP-seq reads at human *CD86* locus in two representative biological replicates of control scramble (Scr) MD901 cells and two representative biological replicates of *CREBBP* KD (sh*CREBBP*) MD901 cells. Shaded areas highlight the regions showing loss of H3K27ac in KD cells. **I,** Pathways analysis of genes ($n = 1147$) with >25% reduction of H3K27ac reads at enhancers in murine VavP-*Bcl2*/sh*Crebbp* tumors, or genes ($n = 2{,}928$) with >25% reduction of H3K27ac reads at enhancers in *CREBBP* knockdown cells. Heat map represents the BH-adjusted *P* value of each gene set tested. **J,** UCSC read-density tracks of normalized BCL6 (purple) and SMRT (orange) ChIP-seq reads in human tonsilar GCBs, H3K27ac ChIP-seq reads in human tonsilar NBCs (red) and GCBs (blue), and H3K27ac ChIP-seq in control scramble (Scr, green) and *CREBBP* KD (sh*CREBBP*, turquoise) MD901 cells at the human MHC II loci. BCL6 and SMRT peaks determined by MACS2 are indicated by gray bars under the read-density track. Shaded areas highlight the enhancers that were bound by BCL6 and SMRT, and showed loss of H3K27ac in *CREBBP* KD cells.

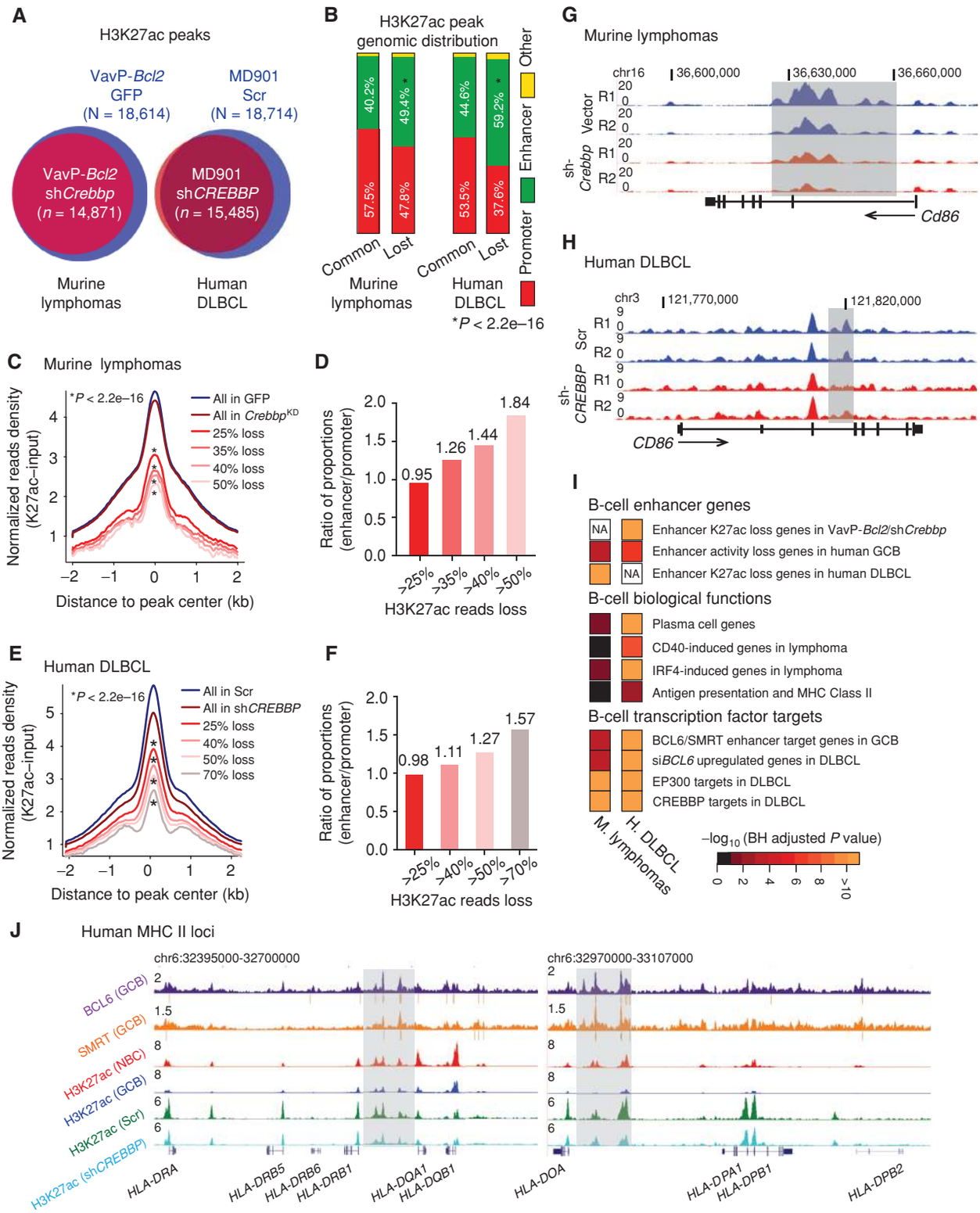

in NBCs, suggesting that BCL6 normally attenuates the MHC II locus during the GC reaction (Fig. 2J). H3K27ac at these enhancers was also reduced by *CREBBP* KD (Fig. 2J; Supplementary Fig. S8). These results indicate novel and opposing functions for BCL6/SMRT complexes and CREBBP in immune recognition.

CREBBP-Mutant Lymphomas Exhibit a GC/BCL6 Target Enhancer Repression Signature

To determine the relevance of these experimental CREBBP signatures to those occurring in the human disease, we next performed RNA-seq and mutation profiling in the DNA of two cohorts of patients with follicular lymphoma (Supplementary Table S3). Nonsynonymous *CREBBP* cSNVs were detected in 38.5% of cohort 1 and 46.1% in cohort 2, mostly clustering to four hotspots in the HAT domain (Supplementary Fig. S9A and S9B; Supplementary Table S4). Somatic mutations were validated by Sanger sequencing in a random subset of tumors and their germline controls (Supplementary Fig. S9C). RNA-seq was also performed in 347 DLBCL patient samples, of which 20.5% (n = 71) carried *CREBBP* mutations that were determined by targeted sequencing of tumor DNA (Supplementary Fig. S9A). *CREBBP* mutations were significantly more frequent in GCB–DLBCL than ABC–DLBCL [P = 1.42E−5, cell-of-origin classification determined by NanoString Lymph2Cx (16); Supplementary Fig. S9D] and again preferentially involved the HAT domain (Supplementary Table S5). We examined differential gene expression between *CREBBP*-mutant and *CREBBP* WT samples lacking other epigenetic mutations that might introduce confounding effects. In all three cohorts, there was a significant skewing toward the genes being more repressed than activated in CREBBP-mutant patients when we examined the top differentially expressed genes (Fig. 3A–C; Supplementary Fig. S10A). Comparison of the signatures of the three cohorts indicated that they were extremely similar [gene-set enrichment analysis (GSEA) FDR $q < 0.05$], confirming that similar genes were affected across patients with *CREBBP*-mutant follicular lymphoma and DLBCL (Supplementary Fig. S10B). The same repressive pattern was induced by *CREBBP* knockdown in human GC–derived DLBCL cell lines (Fig. 3D). Indeed, GSEA also revealed that the follicular lymphoma and DLBCL *CREBBP* mutant repressed signatures were also highly similar to the murine VavP-*Bcl2/Crebbp*^{KD} lymphomas and human *CREBBP* knockdown cell lines (FDR $q < 0.05$, Fig. 3E), demonstrating that these models properly reflect the biology of the human disease, and are furthermore consistent with the fact that HAT domain mutations of *CREBBP* in human patients are known to result in enzymatic loss-of-function (2). In accordance with this notion, genes downregulated in human *CREBBP*-mutant lymphomas were highly significantly enriched for genes that normally lose enhancer H3K27ac in GC B cells, GC exit genes including CD40-induced, IRF4-induced, plasma cell differentiation, and MHC class II antigen processing and presentation (Fig. 3F; for a complete list of enriched pathways, please check Supplementary Table S2). Again, there was significant enrichment for genes with enhancers regulated by BCL6/SMRT complexes, genes induced by *BCL6* siRNA, and the genes that are direct targets of EP300 and CREBBP in DLBCL cells (Fig. 3F). These results identify a conserved signature of CREBBP and BCL6/SMRT–regulated genes that control GC exit and immune recognition.

CREBBP-Mutant Lymphoma Cells are Preferentially Dependent on HDAC3

In normal GC B cells, induction of BCL6 results in the recruitment of the SMRT corepressor and its close homolog NCOR to enhancers, both of which in turn recruit HDAC3. The histone deacetylase HDAC3 is a component of SMRT/NCOR complexes and mediates H3K27 deacetylation of enhancers by BCL6 (17). Thus, BCL6–SMRT/NCOR–HDAC3 complexes "toggle" enhancers that are active in mature B cells likely due to EP300 and CREBBP HAT activity (based on the above data), to a poised H3K27 deacetylated configuration resulting in reduced gene expression (17). This enhancer-repressive effect is reversed when B cells exit the GC reaction through posttranslational modification of SMRT and NCOR and downregulation of BCL6, which results in reacquisition of histone acetylation (18–20). Hence, we hypothesized that a major mechanism through which *CREBBP* mutation/loss-of-function leads to lymphomagenesis is by partially disabling dynamic reversal of enhancer repression mediated by BCL6–SMRT/NCOR–HDAC3 complexes (Fig. 4A).

To first assess the requirement for HDAC3 in mediating BCL6–SMRT/NCOR effects in GC B cells, we performed two experiments. In the first, we obtained mice genetically engineered to simultaneously express mutant forms of NCOR and SMRT that are unable to associate with HDAC3 in a stable manner (21). These mice were immunized with a T-cell–dependent antigen and splenic tissue assessed after 10 days for GC formation. In these animals, we observed an approximately 50% reduction in the abundance of GC B cells as determined by flow cytometry (Supplementary Fig. S11). As this model is constitutive to rule out that this effect could be due to non–B cell–autonomous effects, we next performed a similar experiment in mice engineered for conditional deletion of HDAC3, driven by CD19*Cre*. These mice revealed the same phenotype, with approximately 50% reduction in the abundance of GC B cells after T-cell–dependent antigen stimulation (S.W. Hiebert, data not shown; Fig. 4B). Taken together, these animal models confirm that HDAC3 is required by the BCL6/SMRT complex to fully establish the GC reaction.

Next, to determine whether the opposing effects between CREBBP and BCL6/SMRT complexes on gene expression are driven by HDAC3, we analyzed RNA-seq data obtained from purified FACS-sorted GC B cells from CD19*Cre*/*Hdac3*$^{-/-}$ mice. Genes induced in *Hdac3* knockout GC B cells were strikingly and significantly enriched for genes that are repressed in VavP-*Bcl2/Crebbp*^{KD} lymphomas and in human *CREBBP*-mutant follicular lymphoma and DLBCLs (Fig. 4C–F). Accordingly, we also observed enrichment for the BCL6/SMRT enhancer target genes, enhancers that are repressed in GC B cells, and the class II MHC and antigen presentation gene set among genes induced in CD19*Cre*/*Hdac3*$^{-/-}$ GC B cells (Fig. 4G–I). Hence, HDAC3 antagonizes CREBBP function such that *CREBBP* mutation leads to unopposed HDAC3 activity in GC B cells and lymphomas.

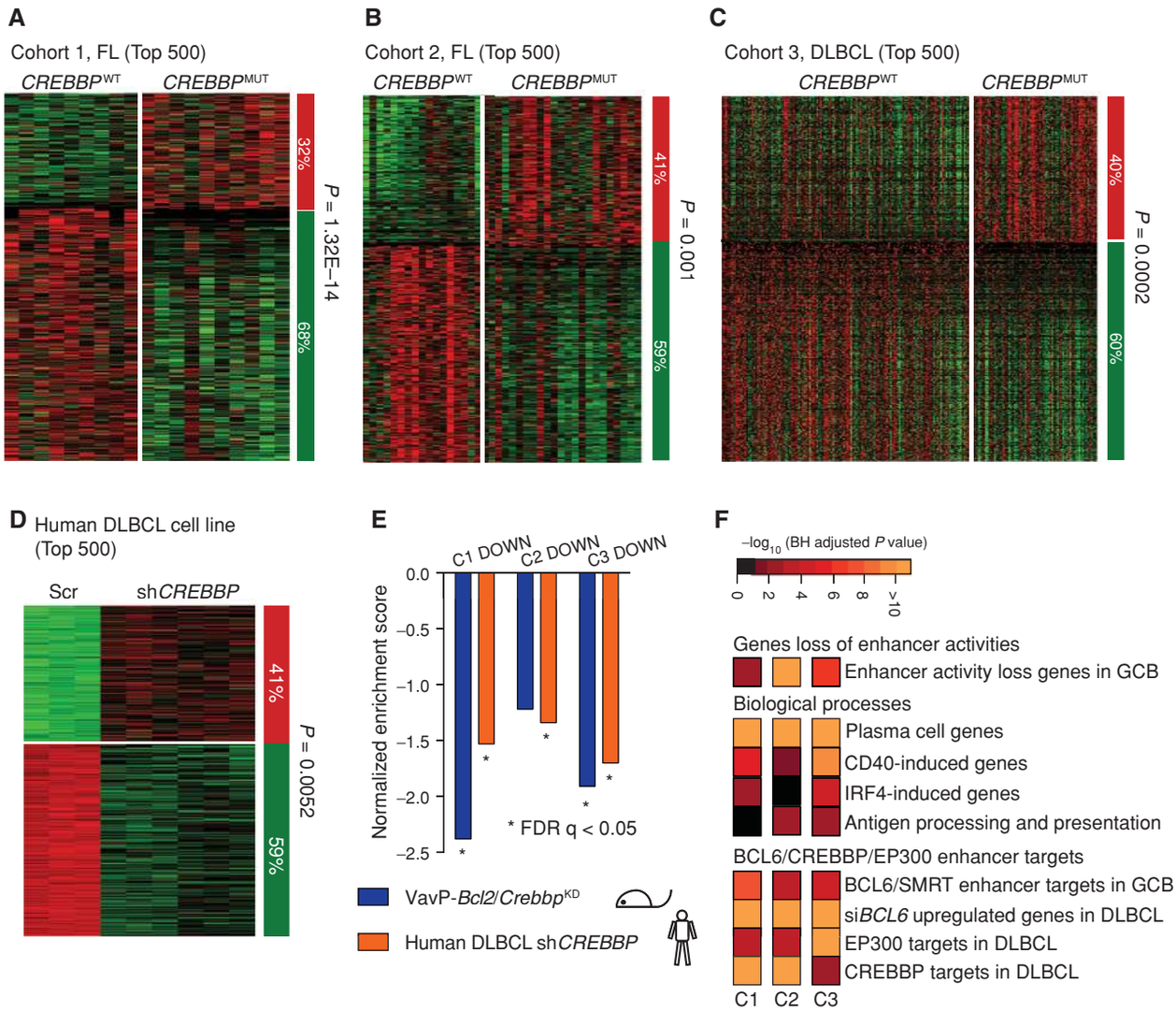

Figure 3. CREBBP loss-of-function results in gene expression repression signature. **A–D,** Supervised analysis of the top 500 most differentially expression genes between *CREBBP* WT (*CREBBP*^{WT}) and mutant (*CREBBP*^{MUT}) follicular lymphoma (FL; **A** and **B**), DLBCL patients (**C**), or between scramble and *CREBBP* knockdown MD901 cells (**D**). Columns represent individual samples, rows correspond to the genes. Heat map represents the z-scores of the expression value (RPKM) characterized by RNA-seq. The column on the right represents the proportion of the genes that were repressed (green) or upregulated (red) in *CREBBP*^{MUT} patient samples as compared with *CREBBP*^{WT} patient samples (**A–C**), or in *CREBBP* knockdown cells as compared with scramble control samples of the respective cohorts (**D**). Statistical significance was determined by Fisher exact test. **E,** Summary of the GSEA of the downregulated genes in the top 500 most differentially expressed genes of respective cohorts as compared with ranked gene expression changes between either murine VavP-*Bcl2*/*Crebbp*^{KD} and VavP-*Bcl2*/EV murine tumors (purple bars) or between *CREBBP* KD and Scr MD901 cells (orange bars). *, significant enrichment (FDR $q < 0.05$). **F,** Pathway analysis of the downregulated genes within the top 500 most differentially expressed genes of respective cohorts. Heat map represents the $-\log_{10}$ BH-adjusted *P* value of each gene set tested.

It is well established that BCL6 maintains the growth of lymphoma cells partly through its recruitment of SMRT/HDAC3 complexes (17). Given that our data suggest that CREBBP loss-of-function particularly strengthens this aspect of BCL6 function, we postulated that *CREBBP*-mutant lymphoma cells would be especially sensitive (to a greater degree than *CREBBP* WT cells) to HDAC3 loss-of-function. We therefore transduced *CREBBP*-mutant and WT DLBCL cells with inducible lentiviral shRNAs against *HDAC3* that exhibited robust knockdown of HDAC3 expression (Supplementary Fig. S12A). *HDAC3* knockdown significantly impaired the proliferation of *CREBBP*-mutant (OZ and RIVA), but not *CREBBP* WT DLBCL cells (Fig. 4J; Supplementary Fig. S12B). *HDAC3* knockdown also caused more apoptosis in *CREBBP*-mutant RIVA cells, but not WT cell lines (Fig. 4K; Supplementary Fig. S12C). We next evaluated the effect of *HDAC3* knockdown in *CREBBP*-mutant and WT DLBCL *in vivo*. We performed this experiment in two ways. First, we enriched the *CREBBP*-mutant (FARAGE) and WT (OCI-Ly7) cells transduced with control shRNA or sh*HDAC3* with a puromycin selection mark, and implanted these cells into SCID mice. We observed that knockdown of *HDAC3*

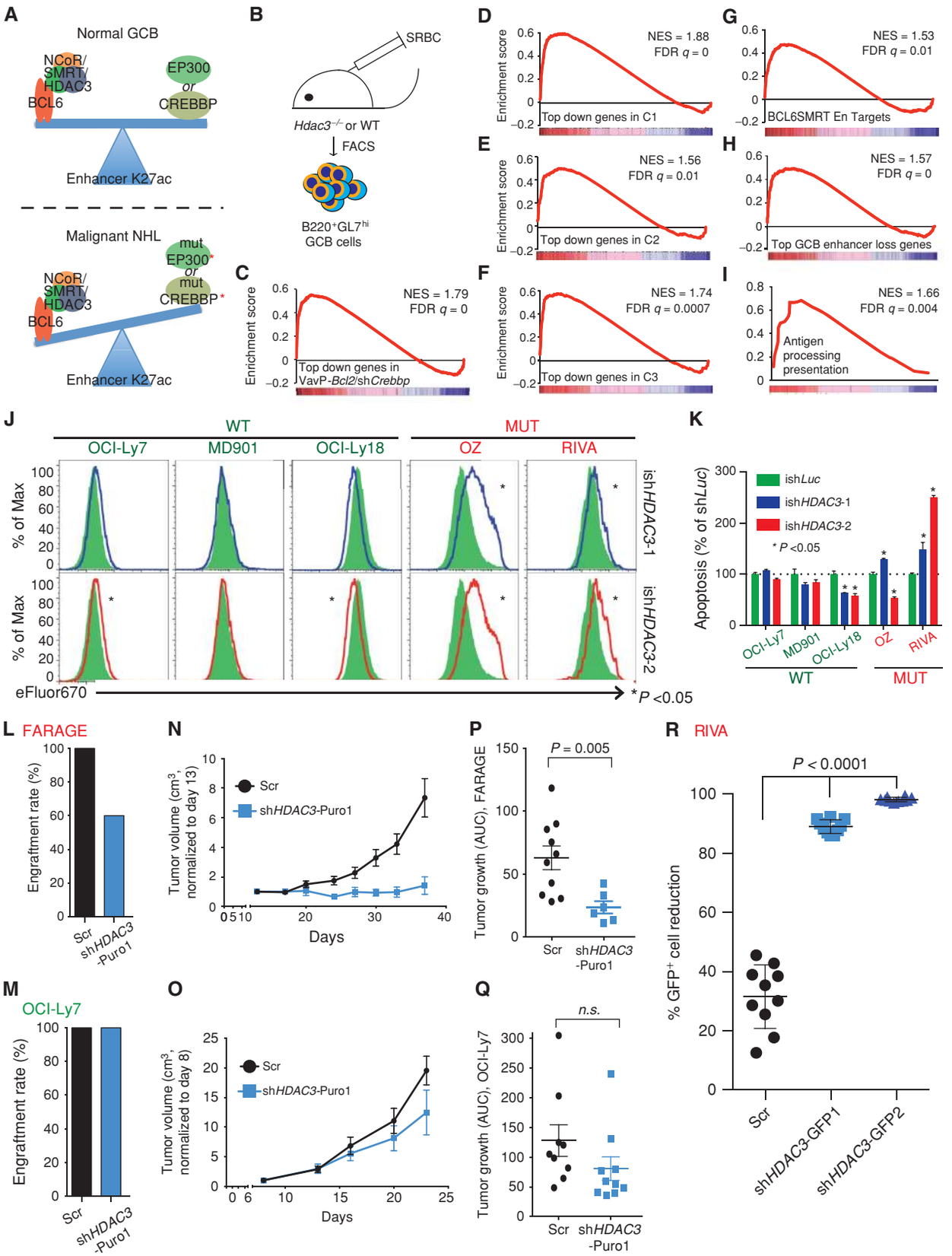

impaired engraftment of *CREBBP*-mutant but not *CREBBP* WT DLBCL cell lines, as compared with control (Fig. 4L and M). Among engrafted mice, *HDAC3* knockdown resulted in much more significant retardation of tumor growth in the *CREBBP*-mutant ($P = 0.005$) than WT DLBCL (Fig. 4N–Q). Immunohistochemical analysis showed a trend toward increased necrotic areas in the *CREBBP*-mutant mice with *HDAC3* knockdown, but no difference in the *CREBBP* WT lymphomas (Supplementary Fig. S12D). Second, we implanted NSG mice with *CREBBP*-mutant RIVA cells containing a mixed population of GFP$^+$ sh*HDAC3* or control shRNA transduced with nontransduced cells. Five weeks after implantation, the mice were sacrificed and lymphomas evaluated to ascertain the percentage of GFP$^+$ cells. *HDAC3* knockdown lymphomas featured almost complete loss of GFP representing a highly significant depletion of GFP$^+$ cells as opposed to control shRNA–transduced cells ($P < 0.0001$, Fig. 4R). Hence, *CREBBP*-mutant DLBCLs are addicted to HDAC3 for their proliferation and survival.

Repression of Antigen Processing and Presentation Genes Due to *CREBBP* Loss Can Be Rescued by HDAC3 Inhibition

Finally, to confirm the opposing actions and potential novel biological effects of CREBBP and HDAC3, we examined in greater detail their counter-regulatory effects at the MHC class II loci, which, as shown above, are counter-regulated by CREBBP and BCL6/SMRT/HDAC3 complexes. First, to confirm that the recruitment of HDAC3 to these loci was dependent on BCL6, we performed HDAC3 ChIP-qPCR in DLBCL cells after transduction with si*BCL6* or control siRNA. *BCL6* siRNA, but not control, induced the expected reduction in BCL6, as well as loss of enrichment of HDAC3 at MHC class II–related loci (Supplementary Fig. S13). Next, we observed that the transduction of *CREBBP* WT DLBCL cells (OCI-Ly18 and MD901) with either of the two *CREBBP* shRNAs induced significant reduction in the transcript abundance of MHC class II genes in these cells (Fig. 5A and B; for primer sequences, see Supplementary Table S6). Furthermore, this gene expression reduction was accompanied by loss of H3K27ac at enhancers of the MHC class II genes (Fig. 5C and D; for primer sequences, see Supplementary Table S6). *CREBBP* knockdown likewise accordingly induced significant reduction of cell surface HLA-DR as detected by flow cytometry in two independent experiments (Fig. 5E–H; Supplementary Fig. S14A and S14B). Notably, the treatment of *CREBBP* knockdown cells with a selective HDAC3 inhibitor (22) rescued the expression of most of these MHC class II genes (Fig. 5A and B) and H3K27ac enrichment at their enhancers (Fig. 5C and D), and restored the expression of cell surface HLA-DR (Fig. 5E–H; Supplementary Fig. S14A and S14B). Consistent with the results from Green and colleagues showing that primary *CREBBP*-mutant DLBCLs less efficiently induced allogeneic T-cell activation (7), we showed that *CREBBP* knockdown cells failed to stimulate human T-cell proliferation to the same extent as control knockdown cells (Fig. 5I and J; Supplementary Fig. S14C). This loss of the T-cell stimulation ability was at least partially rescued by treatment with the selective HDAC3 inhibitor in both cell lines (Fig. 5I and J; Supplementary Fig. S14C). Taken together, our data suggest that in GC B cells, MHC class II gene expression is controlled by enhancer toggling through BCL6/SMRT/HDAC3 complexes in contraposition with CREBBP. *CREBBP* mutation or loss-of-function allows greater BCL6/SMRT/HDAC3–mediated repression, resulting in the reduction of surface expression of these genes and thus potentially impairing the ability of T cells to suppress the outgrowth of malignant B cells.

DISCUSSION

CREBBP is one the most frequently mutated genes in human lymphomas, and our study demonstrates its tumor suppressor action and provides insight into its mechanism. We find that CREBBP loss-of-function disrupts a finely tuned mechanism of enhancer toggling that controls gene expression during the GC reaction. Specifically, CREBBP and likely EP300 maintain H3K27 acetylation of specific enhancers required for the terminal differentiation and immune signaling in mature B cells. This enables B cells to undergo plasma cell differentiation upon immunization. However a subset of B cells follows an alternative fate and instead enters the proliferative and mutagenic GC reaction. In GC B cells, these enhancers are transiently repressed by BCL6/SMRT/HDAC3 complexes through H3K27 deacetylation. This effect is terminated through CD40 signaling that disrupts BCL6/SMRT repression complexes upon GC exit, upon which enhancers recover their H3K27-acetylated active state (18–20).

Figure 4. Loss of *HDAC3* inhibits *CREBBP*-mutant lymphoma growth *in vitro* and *in vivo*. **A,** A schematic model showing the opposing effects on enhancer H3K27ac regulation between CREBBP and EP300 and BCL6/SMRT/HDAC3 corepressor complex in normal GCB cells and in malignant lymphoma (NHL) cells. **B,** A cartoon outlining the generation and collection of GC B cells in *Hdac3*$^{-/-}$ and *Hdac3*$^{fl/fl}$ mice for RNA-seq. SRBC, sheep red blood cell. **C–I,** GSEA enrichment plots showing correlation of different genesets with ranked expression change between murine *Hdac3*$^{-/-}$ and *Hdac3*$^{fl/fl}$ germinal center B cells, $n = 2$ from each group. NES, normalized enrichment score. **J,** Representative flow cytometry histograms demonstrating proliferation of *CREBBP* WT lymphoma cell lines (OCI-Ly7, MD901, and OCI-Ly18) and mutant lymphoma cell lines (OZ and RIVA). Each cell line was transduced with inducible shRNAs against either control Luciferase gene (ish*Luc*, green shaded area) or *HDAC3* (ish*HDAC3*-1, blue, top, and ish*HDAC3*-2, red, bottom). Transduced cells were labeled with cell proliferation dye eFluor 670 and cultured for 5 days in the presence of 0.2 μg/mL doxycycline. *, statistical difference between ish*Luc* ($n = 3$) and respective ish*HDAC3* ($n = 3$), determined by *t* test. **K,** Bar plot showing the relative apoptotic cells in *CREBBP* mutant or WT cells with ish*HDAC3*-1 (blue), and ish*HDAC3*-2 (red) as compared with ish*Luc* (green), measured by Annexin-V staining. The numbers represent mean and SEM of the percentage of Annexin V$^+$/DAPI$^-$ cells of three replicates normalized to the average in the sh*Luc* samples. **L** and **M,** Engraftment rate of FARAGE (L, *CREBBP* mutant) or OCI-Ly7 (M, *CREBBP* WT) in SCID mice. SCID mice were subcutaneously injected with ten million FARAGE or OCI-Ly7 cells either transduced with a scramble shRNA (black) or a shRNA against *HDAC3* (blue), 10 animals per group. **N** and **O,** Tumor growth plots of FARAGE (**N**) and OCI-Ly7 (**O**) xenografted mice. **P** and **Q,** Dot plots showing the growth of each tumor measured as area under the curve. Average tumor growth (mean ± SEM) is represented on the y-axis, which represents tumor volume (cm^3)/time (days). Statistical significance was determined by Mann–Whitney *U* test. **R,** Dot plots showing the percentages of GFP-positive tumor cell population reduction in RIVA xenograft model with either *HDAC3* shRNAs (sh*HDAC3*-GFP1, sh*HDAC3*-GFP2) or scramble shRNA (Scr). For each group, mean ± SD was presented. Statistical significance was calculated by Mann–Whitney test.

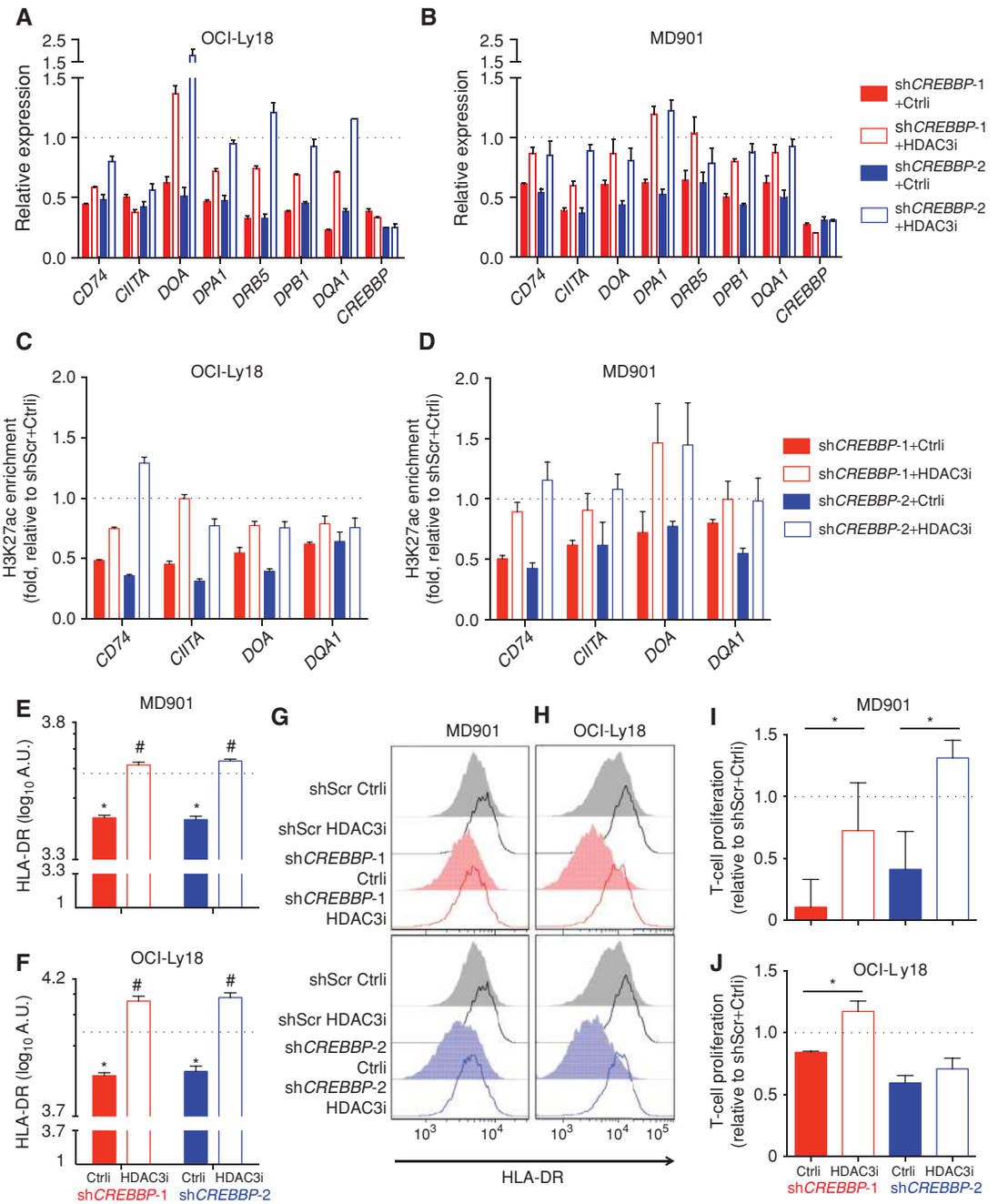

Figure 5. CREBBP regulates antigen processing and presentation gene enhancers. **A** and **B,** Bar plots representing the relative expression of antigen presentation and MHC II genes in OCI-Ly18 (**A**) and MD901 (**B**) cells upon *CREBBP* depletion and treated with either a selective HDAC3 inhibitor (HDAC3i; 20 μmol/L) or a control compound (Ctrli), as compared with scramble shRNA–induced cells (set as 1, dotted lines). Bar graph represents mean and SEM. from three replicates. **C** and **D,** Bar plots representing the relative H3K27ac enrichment at enhancers of MHC II genes in OCI-Ly18 (**C**) and MD901 (**D**) cells upon *CREBBP* depletion and treated with either a selective HDAC3 inhibitor (HDAC3i; 20 μmol/L) or a control compound (Ctrli), as compared with scramble shRNA–induced cells (set as 1, dotted lines). Bar graph represents mean and SEM from three replicates. **E** and **F,** Quantification of HLA-DR measured by flow cytometry in sh*CREBBP* or scramble-transduced lymphoma MD901 (**E**) and OCI-Ly18 (**F**) cells treated with either a selective HDAC3 inhibitor (HDAC3i; 20 μmol/) or a control compound (Ctrli). Cells were transduced with shRNAs for 3 days and then treated with compounds for 96 hours. The data was represented as mean ± SD. Statistical significance was determined by Student *t* test. *, significant difference between control compound-treated scramble or sh*CREBBP*-transduced cells ($P < 0.05$). #, significant difference between control compound and selective HDAC3 inhibitor–treated cells ($P < 0.05$). **G** and **H,** Representative flow cytometry histograms showing cell surface level of MHC II molecule HLA-DR that were quantified in **E** and **F**. **I** and **J,** Bar plots showing the relative proliferation of T cells stimulated by sh*CREBBP* or scramble-transduced lymphoma MD901 (**I**) or OCI-Ly18 (**J**) cells treated with either a selective HDAC3 inhibitor (HDAC3i; 20 μmol/L) or a control compound (Ctrli). The data indicate relative folds of T-cell proliferation, represented as ratio of fluorescence (560 nm/590 nm) from each treatments to that from scramble shRNA–transduced cells treated with control compound (set as 1, dotted lines). Statistical significance was determined by Student *t* test.

However, *CREBBP* mutation results in a failure to reactivate these enhancers, which impairs GC exit and immune recognition programs, and ultimately promotes malignant transformation. Because GC enhancer deacetylation is driven by HDAC3, *CREBBP*-mutant lymphomas become especially dependent on this protein, as observed in our functional assays *in vitro* and *in vivo*. Hence HDAC3 dependency is an exploitable target in patients with lymphoma with *CREBBP* somatic mutations. Because follicular lymphomas and DLBCLs are dependent on BCL6 regardless of *CREBBP* mutation status, it is expected that *CREBBP* WT lymphomas would manifest some degree of HDAC3 dependency as well. Accordingly, our data show that HDAC3 knockdown still has mild deleterious effects in *CREBBP* WT DLBCL cell lines *in vitro* and *in vivo*.

Mutant CREBBP–induced loss of enhancer function is reminiscent of recent findings indicating that somatic mutations of the histone methyltransferase *KMT2D* in B-cell lymphomas induce malignant transformation by disrupting enhancer H3K4 monomethylation and dimethylation (14, 23). In the case of KMT2D, the impact of loss-of-function alleles is to attenuate enhancer response to CD40 and other signaling pathways. Hence, induction of gene expression linked to GC exit signals is dampened and there is aberrant persistence of GCs beyond their usual transient time frame, and affected B cells manifest a defect in class switch recombination (14). Even though KMT2D and CREBBP are both enhancer regulators, they seem to have at least partially distinct functions given that (i) somatic mutation of these two genes often occurs together in DLBCL and follicular lymphoma and (ii) their target genes and downstream biological effects are not identical [e.g., enhanced proliferation in KMT2D (14, 23) or reduced MHC class II expression in CREBBP loss-of-function].

It is important to underline that the transcriptional and epigenetic signatures induced by *CREBBP* knockdown in mice and human cells were highly similar to that of human patients with *CREBBP* mutations. Moreover, the critical mechanistic point of HDAC3 dependency was observed in both *CREBBP*-mutant DLBCL cells as well as CREBBP loss-of-function experiments. Finally, the loss of MHC class II gene expression and loss of the ability of lymphomas to stimulate a T-cell response was similar in *CREBBP* knockdown as well as *CREBBP*-mutant primary patients compared with respective controls (7). These three points confirm the relevance of our findings to the natural process of *CREBBP* somatic mutation. We underline that MHC class II loss-of-function is an important event in lymphomas, associated with inferior clinical outcome (24). Along these lines, it is notable that the BCL6/SMRT/HDAC3/CREBBP mechanism regulates not only enhancers within the MHC class II loci, but also genes that themselves play important roles in supporting MHC class II expression such as *CIITA*, or that enable activity of MHC class II surface proteins such as *CD74*. In addition to being a target gene of BCL6 and CREBBP, *CIITA* itself is mutated in approximately 10% of DLBCLs based on publicly available data from The Cancer Genome Atlas (data not shown), and even more frequently in primary mediastinal large B-cell lymphoma (25). The occurrence of somatic mutations of *CREBBP* and its downstream target *CIITA* in DLBCLs supports the notion that loss-of-function of antigen-presenting functions is an important aspect of lymphomagenesis. Yet we do not rule out that *CREBBP* mutation might have additional functions. For example, it was proposed that *CREBBP* mutation could impair p53 function and enhance BCL6 through reduced acetylation (2). Although the most pronounced loss of H3K27 acetylation occurred at enhancers, we point out that at least part of the function of CREBBP may still be related to effects on promoter function as shown in Supplementary Table S2. Future studies should help to determine whether any other putative effects of CREBBP are relevant to lymphomagenesis beyond those described in this article.

Finally, it is intriguing that the CREBBP–HDAC3 enhancer toggling mechanism controls expression of antigen processing and presentation genes, which could potentially disrupt immunosurveillance by T cells. As noted, *CREBBP*-mutant lymphomas feature less T-cell infiltration and impaired ability to activate T cells *ex vivo* (7). We show that CREBBP loss-of-function indeed directly mediates loss of MHC class II expression and the ability of T cells to recognize B cells. Most strikingly, we show that this effect is rescued by targeting HDAC3. This finding is consistent with and refines the notion that targeting pan-HDAC inhibitors could induce MHC class II expression in lymphoma cells (26). Hence, our findings have direct ramifications for lymphoma therapy, as *CREBBP*-mutant lymphomas may exhibit continued requirement for HDAC3 activity to hide from T cells through epigenetic silencing of MHC class II. Synthetic HDAC3 dependence in *CREBBP*-mutant tumors may thus have dual actions on both immune surveillance and other growth-promoting functions of BCL6/SMRT complexes. These mechanisms indicate an opportunity for HDAC3-specific inhibitors as a precision medicine approach for *CREBBP*-mutant lymphomas.

METHODS

Characterization of Human NHL Samples

Characterization of NHL samples, including two cohorts of follicular lymphoma samples and one cohort of newly diagnosed DLBCL samples, was previously described by Ortega-Molina and colleagues (14). These studies were approved by either the Institutional Review Board (IRB) at Weill Cornell Medical College (WCMC; IRB#0107004999), or the Research Ethics Board at the University of British Columbia, British Columbia Cancer Agency (REB#H13-01478). Informed consent was obtained from all the subjects.

Tonsilar B-cell Isolation

Primary cells were isolated from normal fresh deidentified human tonsillectomy specimens (IRB#0805009767). Naïve B cells were labeled with anti-IgD-FITC followed by anti-FITC Microbeads (MACS). GC B cells were first labeled with anti-CD77 (rat IgM), then mouse anti-rat IgM, IgG1 isotype, and followed with rat anti-mouse IgG1 Microbeads. Bead-labeled cells were then enriched by passing through an autoMACS instrument using the PosselD protocol. The purity of the isolated cells is normally greater than 90%.

Generation of Mice

Animal studies have been approved by Institutional Animal Care and Use Committees at Memorial Sloan Kettering Cancer Center (protocol #: 07-01-002) and WCMC (protocol #: 2011-0034). The vavP-*Bcl2* mouse model of follicular lymphoma (27) was adapted to the adoptive transfer approach using retrovirally transduced HPCs (28). Briefly, VavP-*Bcl2* transgenic HPCs from fetal livers (E14.5) were transduced with retroviruses expressing short hairpin RNAs against *Crebbp* or empty vector,

and the recipients were monitored for 200 days. Eight- to 10-week-old C57BL/6 females were used for all transplantation experiments.

The retroviral vectors are based on MSCV (29). Mouse shRNAs were designed using Designer of Small Interfering RNA.

sh*Crebbp* #1: ATGCATCAGATTTGTGTTCTA
sh*Crebbp* #2: CAGGACCTACGGAGTCATCTA
sh*Crebbp* #3: CTGGTTGCCTATGCTAAGAAA
sh*Ep300* #1: CAGGTACAAGCAAAGAATCAA

Mouse B220$^+$ Tumor Sample Preparation

B220$^+$ cells were purified from mouse lymphomas by immunomagnetic enrichment with CD45R microbeads (Miltenyi Biotec).

Histology

Tissues were fixed overnight in formalin, embedded in paraffin blocks, and sectioned. Tissue sections were stained with hematoxylin/eosin, B220, CD3, Ki67, and TUNEL following standard procedures.

Histologic Score System

Semiquantitative scale of organ infiltration was used on the basis of the size of the infiltrate of atypical lymphocytes, corresponding to 1+ (size of the infiltrate <50% of 40× field); 2+ (size of the infiltrate >50% of 40× and < 100% of 40× field); 3+ (size of the infiltrate > one 40× field) for all organs, except spleen. Splenic infiltrate was evaluated on the basis of the size of the white pulp and atypical lymphocytes outside of the white pulp, as follows: 1+ atypical lymphocytes occupying <60% of spleen surface; 2+ atypical lymphocytes occupying between 60% and 80% of spleen surface; 3+ atypical lymphocytes occupying >80% of spleen surface.

Flow Cytometric Analysis

Mouse tumor cell suspensions were stained as described previously (28). The antibodies used were B220/CD45R (BD Biosciences, 553092, 1:200) or IgG1 (BD Biosciences, 560089, 1:200) conjugated with APC, CD19 (BD Biosciences, 557399, 1:200), IgM (BD Biosciences, 553409, 1:200), IgD (BD Biosciences, 558597, 1:200), GL7 (BD Biosciences, 561530, 1:200) conjugated with phycoerythrin, and analyzed with BD LSRFortessa cell analyzer. Analysis was performed with FlowJo software (Tree Star).

IgVH Rearrangement Analysis

PCR to evaluate IgVH rearrangements was performed on the cDNA of lymphoma cells with a set of forward primers that anneal to the framework region of the most abundantly used IgVH gene families and reverse primers located in the JH1-4 gene segments (30).

Somatic Hypermutation

The genomic sequences from VH to the intron downstream of JH4 were PCR-amplified from cDNA of B220$^+$ cells using degenerate forward primers for the different VH families (31) and a reverse primer (5′-AGGCTCTGAGATCCCTAGACAG-3′; ref. 32) downstream JH4. Proofreading polymerase (Phusion High Fidelity, NEB) was used for amplification with PCR conditions previously published (31). Amplification products were isolated from agarose gel and cloned into pGEMT, and single colonies were submitted to Sanger sequencing. Sequences were compared with IgBLAST (33).

Cell Culture

Human DLBCL cell lines were grown in medium containing either 90% Iscove's Modified Dulbecco's Medium (OCI-Ly1, OCI-Ly7) or 90% RPMI-1640 (FARAGE, MD901, OCI-Ly18, RIVA, OZ), 10% FBS, 1% HEPES, 1% glutamine, and 1% penicillin/streptomycin. OCI-Ly1, OCI-Ly7, and OCI-Ly18 were obtained from Ontario Cancer Institute in June 2011. FARAGE was obtained from the ATCC in May 2011. MD901 was provided by Jose Angel Martinez-Climent [Centre for Applied Medical Research (CIMA), Pamplona, Spain] in June 2011. OCI-Ly1, OCI-Ly7, OCI-Ly18, FARAGE, and MD901 were recently authenticated by Biosynthesis using their STR Profiling and Comparison Analysis Service in February 2015. RIVA and OZ were authenticated by immunophenotyping in October 2016. These cell lines have also been routinely tested for *Mycoplasma* contamination in the laboratory.

Immunoblot Analysis

The protein levels of CREBBP and HDAC3 in whole-cell extracts were detected by Western blotting using rabbit anti-CREBBP (Santa Cruz Biotechnology, sc-369, 1 μg/mL) and rabbit anti-HDAC3 (Santa Cruz Biotechnology, sc-11417, 1 μg/mL), respectively. Levels of H3K27ac were detected by Western blotting using histone extracts collected using the acid extraction method and blotted with rabbit anti-H3K27ac (Abcam, ab4729, 1 μg/mL) and rabbit anti-total H3 (Abcam, ab1791, 1 μg/mL).

Knockdown of Human CREBBP and HDAC3

The shRNA sequences used to knock down *CREBBP* or *HDAC3* expression in human cell lines are as follows: shRNAs against human *CREBBP*:

sh*CREBBP*-1: GTAACTCTGGCCATAGCTTAA
sh*CREBBP*-2: GATGCATCAGATTTGCGTTCT
shRNA against human *HDAC3* used in xenograft experiment
sh*HDAC3*-GFP1 or Puro1 (same vector backbone but with different selection markers):
CCGGCAAGAGTCTTAATGCCTTCAACTCGAGTTGAAGGCATTAAGACTCTTGTTTTTTG
sh*HDAC3*-GFP2:
CCGGGCCTGACAATGGTACCTATTACTCGAGTAATAGGTACCATTGTCAGGCTTTTTTG
Inducible shRNAs against human *HDAC3* used in cell proliferation and apoptosis experiments:
ish*HDAC3*-1:
TGCTGTTGACAGTGAGCGCCCGGGGTTCAAGAAGCTTTCTATAGTGAAGCCACAGATGTATAGAAAGCTTCTTGAACCCCGTTGCCTACTGCCTCGGA
ish*HDAC3*-2:
TGCTGTTGACAGTGAGCGAACCATGACAATGACAAGGAAATAGTGAAGCCACAGATGTATTTCCTTGTCATTGTCATGGTCTGCCTACTGCCTCGGA

mRNA-seq Library Preparation and Sequencing Analysis

Total RNA was extracted from patient samples using TRIzol (LifeTechnologies). RNA concentration was determined using Qubit (LifeTechnologies) and integrity was verified using Agilent 2100 Bioanalyzer (Agilent Technologies). High quality total RNA (100–200 ng) from each sample was subjected to sequencing library preparation following the protocols of either the Illumina TruSeq RNA Kit (human cohort 1) or the TruSeq Stranded Total RNA with Ribo-Zero Kit (human cohort 2, mouse tumors, and MD901 CREBBP KD). Libraries were multiplexed (6 samples per lane) and sequenced on Illumina HiSeq 2500 as either 50-bp single-read runs (TruSeq RNA) or 50-bp paired-end runs (Stranded Total RNA).

Reads were mapped to the reference human (hg19) or mouse (mm10) genome sequence, using Tophat2 aligner (34) with the default parameters. The mRNA expression level for each gene was represented as FPKM, called by Cufflinks (35). For downstream RNA-seq analysis, the comparison of gene expression between two groups was determined by the Student *t* test and the Benjamini–Hochberg adjusted *P* values.

ChIP and ChIP-seq Library Preparation and Sequencing Analysis

Histone ChIPs, including H3K4me1/2, H3K4me3, and H3K27ac ChIPs in human tonsilar naïve and GC B cells, human DLBCL cell

lines, and mouse splenic tumor cells, were performed as described previously (14). BCL6 and HDAC3 ChIP-qPCR as well as BCL6 and SMRT ChIP-seq data were adapted from Hatzi and colleagues (17). Briefly, 1–5 × 10^6 cells were fixed with 1% formaldehyde for 10 minutes at room temperature, followed by nuclei preparation and sonication (Branson Sonicator, Branson or Covaris E220, Covaris) to achieve enrichment of short fragment chromatin (~200 bp). Antibody [1–2 μg; H3K4me1/2, Abcam, ab32356; H3K4me3, Abcam, ab8580; H3K27ac, Abcam, ab4729, all tested using histone-peptide array (Active Motif 13001) for specificity] was added to precleared chromatin lysate and incubated overnight at 4°C. Enriched chromatin was collected by using protein-A beads (Roche) pull-down and subsequent reverse cross-linking and purification. ChIP-seq libraries were prepared from 5–10 ng ChIP DNA following instructions of Illumina TruSeq ChIP Sample Prep Kit. Pooled libraries (6 samples per lane) were then sequenced on Illumina HiSeq 2500 as 50-bp single-end runs.

CREBBP and EP300 ChIP-seq in DLBCL cell line OCI-Ly7 was performed as described previously (17) with modifications. Briefly, 2 × 10^7 cells were fixed first with 2 mmol/L of disuccinimidyl glutarate (DSG, ProteoChem, C1104) for 45 minutes at room temperature, followed by 1% formaldehyde for 10 minutes at room temperature. Fragmentation of fixed chromatin was performed by sonication of nuclei (Branson Sonicator, Branson) to achieve enrichment of short fragment chromatin (100–500 bp). Antibody (CREBBP, Santa Cruz Biotechnology, sc-369; EP300, Santa Cruz Biotechnology, sc-584; 5 μg) conjugated with Dynabeads protein A (Thermo Fisher Scientific) was added to precleared chromatin lysate and incubated overnight at 4°C. Enriched chromatin was isolated through extensive wash steps and subsequent reverse cross-linking and purification. ChIP-seq libraries were prepared from 5–10 ng ChIP DNA following the instructions of Illumina TruSeq ChIP Sample Prep Kit. Libraries were then sequenced on Illumina HiSeq 2500 as 50-bp single-end runs.

Single-end reads were mapped to the reference human (hg18) or mouse (mm10) genome, using BWA aligner (36) with the default parameters. Only reads mapping uniquely to the genome with not more than 2 mismatches were retained for downstream analysis. Peak detection in each sample was performed with the ChIPseeqer program (37) and annotated to genes and/or promoters based on hg18 or mm10 refseq genes.

The consensus peaks from mouse H3K27ac ChIP-seq for the normal and tumor samples were defined by the overlapping peaks which appear in ≥3 of the 4 normal samples, and ≥4 of the 6 tumors samples (sh*Crebbp*), respectively. The consensus peaks from MD901 H3K27ac ChIP-seq for the scramble shRNA (control) and sh*CREBBP* samples were defined by the overlapping peaks which appear in ≥2 of the 3 samples for the control, and 4 of 6 samples for sh*CREBBP* (i.e., 2/3 samples for both shRNA, or 3/3 samples for one shRNA and 1/3 samples for the other shRNA), respectively.

Pathway Analysis

The pathway analysis was performed as published previously (38). Briefly, the gene sets for canonical pathways and Gene Ontology (GO) terms were downloaded from the Molecular Signatures Database (MSigDB; ref. 39) using C5 collection. The B-cell and lymphoid-specific signatures were curated by Staudt laboratory (downloaded from ref. 40) or Melnick laboratory from previous publications. This database contains approximately 250 gene sets/signatures associated with normal lymphoid biology and lymphoid neoplasms. For the complete list of pathways, please check Supplementary Table S1. The Fisher exact test was used to calculate enrichment *P* values for each of those gene sets and the BH method (41) was used for false discovery rate (FDR) control.

Gene-Set Enrichment Analysis

All the GSEA results in this article were generated from GSEA preranked mode (39). The input files are all the genes and their gene expression level logFC (log2 fold-change) from each RNA-seq dataset, including (i) the three follicular lymphoma or DLBCL patient cohorts (*CREBBP* mutation vs. WT), and (ii) the shRNA data for the mouse or human MD901 cell line (sh*Crebbp* vs. scramble shRNA). All the gene sets used in GSEA were curated by the Staudt laboratory (40) or Melnick laboratory from previous publications.

Mutation Discovery

Exome sequencing of cohort 1 using Aglient SureSelect^{XT}Human All Exon 50 MB Target Enrichment System for Illumina Paired-End Sequencing Library Kit (Agilent Technologies), Raindance targeted resequencing of cohort 2 (RainDance Technologies), targeted resequencing of cohort 3 (347 tumor samples and 67 matched normal samples), cell-of-origin calling of cohort 3 by Lymph2Cx 20-gene GEP assay on the NanoString platform (NanoString Technologies), as well as mutational calling algorithms were described previously in Ortega-Molina and colleagues (14). Aglient Exome and Raindance platforms were cross-validated using DNA from DLBCL cell lines. More than 95% concordance was observed. Cohort 3 DLBCL targeted resequencing results were further validated by the Fluidigm Access Array system (Fluidigm Corporation).

NS-DAD Animal and Experiment

NS-DAD mice were a generous gift from Dr. Mitchell Lazar (21). Age- and sex-matched mice were immunized intraperitoneally with 0.5 mL of a 2% sheep red blood cell (SRBC) suspension in PBS (Cocalico Biologicals) and sacrificed after 10 days. For staining of GC B-cell populations, single-cell suspensions from mouse spleens were stained using the following fluorescent-labeled anti-mouse antibodies: PE-Cy7–conjugated anti-B220, APC-conjugated anti-B220, PE-conjugated anti-FAS, and APC-conjugated anti-CD38. DAPI was used for the exclusion of dead cells.

Cell Proliferation Assay

After DLBCL cell lines transduced with inducible shRNAs against Luciferase gene (*Luc*, control) and human *HDAC3* (ish*HDAC3*-1, ish*HDAC3*-2) were treated with 0.2 μg/mL doxycycline for 24 hours, cells were labeled with 2.5 μmol/L Cell Proliferation Dye eFluor 670 (eBioscience, 65-0840) and cultured for additional 5 days. The fluorescence intensity of the dye (APC channel) in the GFP$^+$ (FITC channel) cells was measured by flow cytometry right after labeling and every 24 hours subsequently until the end of the experiment.

DLBCL Xenotransplant Models

Ten million puromycin-selected, scramble, or *HDAC3* shRNA–transduced human DLBCL cells (FARAGE or OCI-Ly7) were subcutaneously injected in the left flank of 8-week-old SCID mice. Tumor volume was monitored every 3–4 days using electronic digital callipers (Thermo Fisher Scientific) in two dimensions when tumors became palpable. Mice were sacrificed by cervical dislocation under anesthesia at the end of the experiment when tumors in the scramble shRNA group reached maximum size allowed by the animal protocol.

Fifteen million of either scramble or *HDAC3* shRNA–transduced human DLBCL RIVA cells were subcutaneously injected in the flank of 8-week-old NSG mice. The shRNA vector in this experiment contains a GFP marker. The GFP$^+$ cell percentage before injection was measured by flow cytometry. Tumor volume was monitored every 3–4 days using electronic digital calipers in two dimensions when they became palpable. Mice were sacrificed by cervical dislocation under anesthesia at the end of the experiment when tumors in the scramble shRNA group reached maximum size allowed by the animal protocol. Single-cell suspension was prepared from individual tumor and was stained with anti-human CD19-PE (BD Biosciences, 555413) antibody and DAPI to determine the percentage of GFP$^+$ cells in the CD19-positive human B-cell population by flow cytometry.

siRNA Transfections

OCI-Ly1 cells were transfected using Nucleofector 96-well Shuttle system (Lonza) with 1 μmol/L siRNA against *BCL6* (HSS100968) or nontargeted siRNA (46-2001; Stealth RNAi, Invitrogen).

- si*BCL6*: 5′-CCAUUGUGAGAAGUGUAACCUGCAU-3′

Mixed Lymphocyte Reaction

MD901 and OCI-Ly18 B-lymphoblastoid cell lines (BLCL) were transduced with scramble or *CREBBP* shRNAs for 3 days and then treated with a selective HDAC3 inhibitor (20 μmol/L) or a control compound for 96 hours. BLCLs were irradiated (9,000r ^{131}Cs) and added to 1.5×10^5 $CD3^+$ T cells at a ratio of 10:1 T:BLCL in triplicate flat-bottom microwells. Cells were incubated for 5 days at 37°C 5% CO_2, after which T-cell proliferation was assessed by CellTiter Blue Assay (Promega G8081).

Statistical Analysis

Sample sizes for comparisons between cell types or between mouse genotypes followed Mead's recommendations (42). Samples were allocated to their experimental groups according to their predetermined type (i.e., mouse genotype) and, therefore, there was no randomization. Investigators were not blinded to the experimental groups unless indicated. In the case in Fig. 1A, only mice that developed lymphomas were considered; mice that did not develop lymphomas were censored and indicated with ticks in the Kaplan–Meier curves. Survival in mouse experiments was represented with Kaplan–Meier curves, and significance was estimated with the log-rank test. For contingency analysis, we used the χ^2 exact test.

Data Deposition

The RNA-seq and ChIP-seq data are available at the Gene Expression Omnibus database (SuperSeries: GSE79686; MD901 H3K27ac ChIP-seq: GSE79639; MD901 RNA-seq: GSE79684; mouse H3K27ac ChIP-seq: GSE79640; mouse RNA-seq: GSE79685).

Disclosure of Potential Conflicts of Interest

E. Holson reports receiving a commercial research grant from, has ownership interest (including patents) in, and is a consultant/advisory board member for KDAc Therapeutics. R.D. Gascoyne has received speakers bureau honoraria from Seattle Genetics and is a consultant/advisory board member for Celgene and Seattle Genetics. A.M. Melnick reports receiving commercial research support from Janssen, GSK, Roche, and Eli Lilly, and is a consultant/advisory board member for Epizyme. No potential conflicts of interest were disclosed by the other authors.

Authors' Contributions

Conception and design: Y. Jiang, A. Ortega-Molina, K. Hatzi, A.S. Doane, J.E. Kranz, E. Holson, H.-G. Wendel, A.M. Melnick
Development of methodology: Y. Jiang, A.S. Doane, X. Agirre, J.W. Young, A.M. Melnick
Acquisition of data (provided animals, acquired and managed patients, provided facilities, etc.): Y. Jiang, A. Ortega-Molina, H.-Y. Ying, K. Hatzi, S. Parsa, D. McNally, D. Poloway, S. Wang, D. Ennishi, D.W. Scott, K.R. Stengel, S. Sharma, J.W. Young, C.-S. Chu, R. Shaknovich, R.D. Gascoyne, W. Tam
Analysis and interpretation of data (e.g., statistical analysis, biostatistics, computational analysis): Y. Jiang, A. Ortega-Molina, H. Geng, H.-Y. Ying, K. Hatzi, S. Parsa, D. McNally, A.S. Doane, X. Agirre, M. Teater, C. Meydan, Z. Li, S. Wang, D. Ennishi, D.W. Scott, E. Holson, J.W. Young, C.-S. Chu, R.G. Roeder, R. Shaknovich, S.W. Hiebert, R.D. Gascoyne, O. Elemento, H.-G. Wendel, A.M. Melnick
Writing, review, and/or revision of the manuscript: Y. Jiang, A. Ortega-Molina, H.-Y. Ying, K. Hatzi, A.S. Doane, M. Teater, J.W. Young, C.-S. Chu, S.W. Hiebert, R.D. Gascoyne, W. Tam, H.-G. Wendel, A.M. Melnick
Administrative, technical, or material support (i.e., reporting or organizing data, constructing databases): D. McNally, L. Wang, J.E. Kranz, S. Sharma, J.W. Young, H.-G. Wendel
Study supervision: Y. Jiang, J.W. Young, O. Elemento, H.-G. Wendel, A.M. Melnick
Other (provided small molecules used in study): E. Holson

Acknowledgments

We thank the members in the Melnick and the Wendel groups for thoughtful discussions related to this study. We thank the Weill Cornell Medical College Epigenomics core for performing the next-generation sequencing (NGS) library preparation and sequencing for this study, the Rockefeller University Genomics Resource Center for performing NGS of CREBBP/EP300 ChIP for this study. We also thank the members of the Memorial Sloan Kettering (MSK) Antitumor assessment core, the MSK Laboratory of Comparative Pathology, the Weill Cornell Cell Sorting core, the Weill Cornell Leukemia Biorepository and Personalized Medicine Centre, the MSK Flow Cytometry core, and the MSK Molecular Cytology core. We also thank Dr. Mitch Lazar from University of Pennsylvania for providing the NS-DAD mouse model.

Grant Support

Y.Jiang was a Scholar of the American Society of Hematology. A. Ortega-Molina is supported by funding from The Leukemia & Lymphoma Society. H. Geng is supported by a Junior Investigator award from the UCSF Academic Senate. H.-Y. Ying is supported by the 2016 AACR-Takeda Oncology Fellowship in Lymphoma Research (grant number 16-40-38-YING), and was supported by the Ministry of Science and Technology, Republic of China. S. Wang is supported by a postdoctoral fellowship from the Swedish Research Council (VR) and by the 2015 AACR-Millennium Fellowship in Lymphoma Research (grant number 15-40-38-WANG). D. Ennishi, D.W. Scott, and R.D. Gascoyne are supported by a Terry Fox Program Project grant (grant number 1023). D.W. Scott is also funded by the BC Cancer Foundation. S. Sharma and J.W. Young are supported by P01 CA23766 from the National Cancer Institute, NIH and Swim Across America. C.-S. Chu was supported by a fellowship from the Ministry of Science and Technology, Republic of China. R.G. Roeder was supported by NIH grant R01CA178765. O. Elemento is supported by NSF CAREER and R01 CA194547. S.W. Hiebert is supported by NCIR01-CA164605. H.G. Wendel is supported by the American Cancer Society grant RSG-13-048-01-LIB, the Lymphoma Research Foundation, Cycle for Survival, Functional Genomics Initiative, W.H. Goodwin and A. Goodwin and the Commonwealth Foundation for Cancer Research, Steven Greenberg, the Center for Experimental Therapeutics at Memorial Sloan Kettering Cancer Center, NIH grants RO1CA183876-01 and 1R01CA19038-01 and Core Grant P30 CA008748 and P50 CA192937-01A1. H.G. Wendel is a Scholar of the Leukemia and Lymphoma Society and is supported by an LLS SCOR. A.M. Melnick is supported by NIHR01 CA187109, LLS TRP 6457-15, LLS SCOR#7012-16, and the Chemotherapy Foundation.

The costs of publication of this article were defrayed in part by the payment of page charges. This article must therefore be hereby marked *advertisement* in accordance with 18 U.S.C. Section 1734 solely to indicate this fact.

Received September 1, 2016; revised October 11, 2016; accepted October 11, 2016; published OnlineFirst October 12, 2016.

REFERENCES

1. Al-Tourah AJ, Gill KK, Chhanabhai M, Hoskins PJ, Klasa RJ, Savage KJ, et al. Population-based analysis of incidence and outcome of transformed non-Hodgkin's lymphoma. J Clin Oncol 2008;26:5165–9.
2. Pasqualucci L, Dominguez-Sola D, Chiarenza A, Fabbri G, Grunn A, Trifonov V, et al. Inactivating mutations of acetyltransferase genes in B-cell lymphoma. Nature 2011;471:189–95.

3. Pasqualucci L, Trifonov V, Fabbri G, Ma J, Rossi D, Chiarenza A, et al. Analysis of the coding genome of diffuse large B-cell lymphoma. Nat Genet 2011;43:830–7.
4. Lohr JG, Stojanov P, Lawrence MS, Auclair D, Chapuy B, Sougnez C, et al. Discovery and prioritization of somatic mutations in diffuse large B-cell lymphoma (DLBCL) by whole-exome sequencing. Proc Natl Acad Sci U S A 2012;109:3879–84.
5. Zhang J, Grubor V, Love CL, Banerjee A, Richards KL, Mieczkowski PA, et al. Genetic heterogeneity of diffuse large B-cell lymphoma. Proc Natl Acad Sci U S A 2013;110:1398–403.
6. Morin RD, Mendez-Lago M, Mungall AJ, Goya R, Mungall KL, Corbett RD, et al. Frequent mutation of histone-modifying genes in non-Hodgkin lymphoma. Nature 2011;476:298–303.
7. Green MR, Kihira S, Liu CL, Nair RV, Salari R, Gentles AJ, et al. Mutations in early follicular lymphoma progenitors are associated with suppressed antigen presentation. Proc Natl Acad Sci U S A 2015;112:E1116–25.
8. Heintzman ND, Hon GC, Hawkins RD, Kheradpour P, Stark A, Harp LF, et al. Histone modifications at human enhancers reflect global cell-type-specific gene expression. Nature 2009;459:108–12.
9. Creyghton MP, Cheng AW, Welstead GG, Kooistra T, Carey BW, Steine EJ, et al. Histone H3K27ac separates active from poised enhancers and predicts developmental state. Proc Natl Acad Sci U S A 2010;107:21931–6.
10. Lunning MA, Green MR. Mutation of chromatin modifiers; an emerging hallmark of germinal center B-cell lymphomas. Blood Cancer J 2015;5:e361.
11. Loeffler M, Kreuz M, Haake A, Hasenclever D, Trautmann H, Arnold C, et al. Genomic and epigenomic co-evolution in follicular lymphomas. Leukemia 2015;29:456–63.
12. Oricchio E, Nanjangud G, Wolfe AL, Schatz JH, Mavrakis KJ, Jiang M, et al. The Eph-receptor A7 is a soluble tumor suppressor for follicular lymphoma. Cell 2011;147:554–64.
13. Beguelin W, Popovic R, Teater M, Jiang Y, Bunting KL, Rosen M, et al. EZH2 is required for germinal center formation and somatic EZH2 mutations promote lymphoid transformation. Cancer Cell 2013;23:677–92.
14. Ortega-Molina A, Boss IW, Canela A, Pan H, Jiang Y, Zhao C, et al. The histone lysine methyltransferase KMT2D sustains a gene expression program that represses B cell lymphoma development. Nat Med 2015;21:1199–208.
15. Basso K, Dalla-Favera R. Germinal centres and B cell lymphomagenesis. Nat Rev Immunol 2015;15:172–84.
16. Scott DW, Wright GW, Williams PM, Lih CJ, Walsh W, Jaffe ES, et al. Determining cell-of-origin subtypes of diffuse large B-cell lymphoma using gene expression in formalin-fixed paraffin-embedded tissue. Blood 2014;123:1214–7.
17. Hatzi K, Jiang Y, Huang C, Garrett-Bakelman F, Gearhart MD, Giannopoulou EG, et al. A hybrid mechanism of action for BCL6 in B cells defined by formation of functionally distinct complexes at enhancers and promoters. Cell Rep 2013;4:578–88.
18. Polo JM, Ci W, Licht JD, Melnick A. Reversible disruption of BCL6 repression complexes by CD40 signaling in normal and malignant B cells. Blood 2008;112:644–51.
19. Saito M, Gao J, Basso K, Kitagawa Y, Smith PM, Bhagat G, et al. A signaling pathway mediating downregulation of BCL6 in germinal center B cells is blocked by BCL6 gene alterations in B cell lymphoma. Cancer Cell 2007;12:280–92.
20. Ranuncolo SM, Polo JM, Dierov J, Singer M, Kuo T, Greally J, et al. Bcl-6 mediates the germinal center B cell phenotype and lymphomagenesis through transcriptional repression of the DNA-damage sensor ATR. Nat Immunol 2007;8:705–14.
21. You SH, Lim HW, Sun Z, Broache M, Won KJ, Lazar MA. Nuclear receptor co-repressors are required for the histone-deacetylase activity of HDAC3 invivo. Nat Struct Mol Biol 2013;20:182–7.
22. Wagner FF, Lundh M, Kaya T, McCarren P, Zhang YL, Chattopadhyay S, et al. An isochemogenic set of inhibitors to define the therapeutic potential of histone deacetylases in beta-cell protection. ACS Chem Biol 2016;11:363–74.
23. Zhang J, Dominguez-Sola D, Hussein S, Lee JE, Holmes AB, Bansal M, et al. Disruption of KMT2D perturbs germinal center B cell development and promotes lymphomagenesis. Nat Med 2015;21:1190–8.
24. Rimsza LM, Roberts RA, Miller TP, Unger JM, LeBlanc M, Braziel RM, et al. Loss of MHC class II gene and protein expression in diffuse large B-cell lymphoma is related to decreased tumor immunosurveillance and poor patient survival regardless of other prognostic factors: a follow-up study from the Leukemia and Lymphoma Molecular Profiling Project. Blood 2004;103:4251–8.
25. Mottok A, Woolcock B, Chan FC, Tong KM, Chong L, Farinha P, et al. Genomic alterations in CIITA are frequent in primary mediastinal large B cell lymphoma and are associated with diminished MHC class II expression. Cell Rep 2015;13:1418–31.
26. Cycon KA, Mulvaney K, Rimsza LM, Persky D, Murphy SP. Histone deacetylase inhibitors activate CIITA and MHC class II antigen expression in diffuse large B-cell lymphoma. Immunology 2013;140:259–72.
27. Egle A, Harris AW, Bath ML, O'Reilly L, Cory S. VavP-Bcl2 transgenic mice develop follicular lymphoma preceded by germinal center hyperplasia. Blood 2004;103:2276–83.
28. Wendel HG, De Stanchina E, Fridman JS, Malina A, Ray S, Kogan S, et al. Survival signalling by Akt and eIF4E in oncogenesis and cancer therapy. Nature 2004;428:332–7.
29. Dickins RA, Hemann MT, Zilfou JT, Simpson DR, Ibarra I, Hannon GJ, et al. Probing tumor phenotypes using stable and regulated synthetic microRNA precursors. Nat Genet 2005;37:1289–95.
30. Hanna J, Markoulaki S, Schorderet P, Carey BW, Beard C, Wernig M, et al. Direct reprogramming of terminally differentiated mature B lymphocytes to pluripotency. Cell 2008;133:250–64.
31. Ehlich A, Martin V, Muller W, Rajewsky K. Analysis of the B-cell progenitor compartment at the level of single cells. Curr Biol 1994;4:573–83.
32. Gostissa M, Bianco JM, Malkin DJ, Kutok JL, Rodig SJ, Morse HC III, et al. Conditional inactivation of p53 in mature B cells promotes generation of nongerminal center-derived B-cell lymphomas. Proc Natl Acad Sci U S A 2013;110:2934–9.
33. Ye J, Ma N, Madden TL, Ostell JM. IgBLAST: an immunoglobulin variable domain sequence analysis tool. Nucleic Acids Res 2013;41:W34–40.
34. Kim D, Pertea G, Trapnell C, Pimentel H, Kelley R, Salzberg SL. TopHat2: accurate alignment of transcriptomes in the presence of insertions, deletions and gene fusions. Genome Biol 2013;14:R36.
35. Trapnell C, Williams BA, Pertea G, Mortazavi A, Kwan G, van Baren MJ, et al. Transcript assembly and quantification by RNA-Seq reveals unannotated transcripts and isoform switching during cell differentiation. Nat Biotechnol 2010;28:511–5.
36. Li H, Durbin R. Fast and accurate short read alignment with Burrows-Wheeler transform. Bioinformatics 2009;25:1754–60.
37. Giannopoulou EG, Elemento O. An integrated ChIP-seq analysis platform with customizable workflows. BMC Bioinformatics 2011;12:277.
38. Geng H, Brennan S, Milne TA, Chen WY, Li Y, Hurtz C, et al. Integrative epigenomic analysis identifies biomarkers and therapeutic targets in adult B-acute lymphoblastic leukemia. Cancer Discov 2012;2:1004–23.
39. Subramanian A, Tamayo P, Mootha VK, Mukherjee S, Ebert BL, Gillette MA, et al. Gene set enrichment analysis: a knowledge-based approach for interpreting genome-wide expression profiles. Proc Natl Acad Sci U S A 2005;102:15545–50.
40. Shaffer AL, Wright G, Yang L, Powell J, Ngo V, Lamy L, et al. A library of gene expression signatures to illuminate normal and pathological lymphoid biology. Immunol Rev 2006;210:67–85.
41. Benjamini Y, Hochberg Y. Controlling the false discovery rate: a practical and powerful approach to multiple testing. J R Stat Soc Series B Stat Methodol 1995;57:289–300.
42. Festing MFW, Overend P, Gaines Das R, Cortina-Borja M, Berdoy M, et al. The design of animal experiments: reducing the use of animals in research through better experimental design. London: Royal Society of Medicine; 2002.